AGU PUBLICATIONS

Geophysical Research Letters

RESEARCH LETTER
10.1002/2013GL059159

Key Points:
- Airborne in situ measurements in the UTLS were performed with HALO
- Stratospheric tracer correlations are used to quantify mixing in the UTLS
- The stratospheric content relative to the tropopause is investigated

Correspondence to:
T. Jurkat,
tina.jurkat@dlr.de

Citation:
Jurkat, T., et al. (2014), A quantitative analysis of stratospheric HCl, HNO_3, and O_3 in the tropopause region near the subtropical jet, *Geophys. Res. Lett.*, *41*, 3315–3321, doi:10.1002/2013GL059159.

Received 30 DEC 2013
Accepted 3 MAR 2014
Accepted article online 12 MAR 2014
Published online 14 MAY 2014

A quantitative analysis of stratospheric HCl, HNO_3, and O_3 in the tropopause region near the subtropical jet

T. Jurkat[1], C. Voigt[1,2], S. Kaufmann[1,2], A. Zahn[3], M. Sprenger[4], P. Hoor[2], H. Bozem[2], S. Müller[2], A. Dörnbrack[1], H. Schlager[1], H. Bönisch[5], and A. Engel[5]

[1]Deutsches Zentrum für Luft- und Raumfahrt, Institut für Physik der Atmosphäre, Oberpfaffenhofen, Germany, [2]Institut für Physik der Atmosphäre, Johannes Gutenberg-Universität Mainz, Mainz, Germany, [3]Institute for Meteorology and Climate Research, Karlsruhe Institute of Technology, Karlsruhe, Germany, [4]Institute for Atmospheric and Climate Science, Swiss Federal Institute of Technology Zurich, Zurich, Switzerland, [5]Institute for Atmospheric and Environmental Sciences, Goethe Universität Frankfurt, Frankfurt, Germany

Abstract The effects of chemical two-way mixing on the Extratropical Transition Layer (ExTL) near the subtropical jet are investigated by stratospheric tracer-tracer correlations. To this end, in situ measurements were performed west of Africa (25–32°N) during the Transport and Composition of the Upper Troposphere Lower Stratosphere (UTLS)/Earth System Model Validation (TACTS/ESMVal) mission in August/September 2012. The Atmospheric chemical Ionization Mass Spectrometer sampling HCl and HNO_3 was for the first time deployed on the new German High Altitude and Long range research aircraft (HALO). Measurements of O_3, CO, European Centre for Medium-Range Weather Forecasts (ECMWF) analysis, and the tight correlation of the unambiguous tracer HCl to O_3 and HNO_3 in the lower stratosphere were used to quantify the stratospheric content of these species in the ExTL. With increasing distance from the tropopause, the stratospheric content increased from 10% to 100% with differing profiles for HNO_3 and O_3. Tropospheric fractions of 20% HNO_3 and 40% O_3 were detected up to a distance of 30 K above the tropopause.

1. Introduction

Dynamical and chemical processes modify the ozone (O_3) budget of the upper troposphere/lowermost stratosphere (UT/LMS) and lead to locally variable O_3 trends. In this region, O_3 has steep gradients and acts as a strong greenhouse gas with a positive radiative forcing (RF) depending on its location with respect to the tropopause. Only few models explicitly discuss the uncertainty of mixing parametrization and its effect on the RF. They emphasize that small changes in O_3 result in large changes in RF at the tropopause [*Riese et al.*, 2012]. However, understanding of UT/LMS O_3 trends still remains incomplete [*World Meteorological Organization (WMO)*, 2010].

Similar to O_3, nitric acid (HNO_3) shows steep gradients at the tropopause with low concentrations in the upper troposphere and a steady increase in the lower stratosphere. After downward transport into the troposphere, the predominant removal process is particle interaction with subsequent wash out or dry deposition [*Murphy et al.*, 1993]. In addition to the stratospheric contribution, upper tropospheric HNO_3 can be formed in situ from biomass burning plumes, lightning, or aviation. The relative contribution of each source is globally highly variable and therefore difficult to quantify. Next to photochemical production and dry and wet deposition, mixing is an important part of irreversible distribution of tracers, driven by horizontal strain and vertical shear.

The Extratropical Transition Layer is a region of air with mixed tropospheric and stratospheric characteristics centered around the thermal tropopause and has been described extensively using tracer-tracer correlations of carbon monoxide (CO), O_3, and water vapor (H_2O) [*Fischer et al.*, 2000; *Hoor et al.*, 2004; *Hegglin et al.*, 2009]. Tropospheric intrusions transporting low ozone from lower latitudes are known to ventilate the lower stratosphere above the subtropical jet [*Pan et al.*, 2009]. During summer, the weaker isentropic potential vorticity (PV) gradient in the region of the subtropical jet (STJ) allows for a stronger mixing [*Haynes and Shuckburgh*, 2000].

Due to similar source regions at altitudes above 20 km and long chemical lifetimes in the lower stratosphere, in the order of months, it has been suggested that the correlation of the stratospheric tracer hydrogen chloride (HCl) with O_3 can be used to quantify stratospheric O_3 in the upper troposphere [*Marcy et al.*,

2004]. While it is the main chlorine reservoir gas in the stratosphere, HCl has a low tropospheric background, thus being an ideal tracer to study quantitative mixing of trace gases with both tropospheric and stratospheric sources.

Due to the steep gradients at the tropopause, highly resolved measurements of HNO_3, O_3, and HCl are needed. To this end, we performed in situ measurements of HCl and HNO_3 with a newly developed Atmospheric chemical Ionization Mass Spectrometer (AIMS) during the first atmospheric science HALO mission TACTS/ESMVal in August/September 2012. High spatial and temporal resolution of the trace gas measurements allow a good characterization of mixing near the tropopause.

This paper discusses the benefits and limitations of using the relation between stratospheric tracers to study mixing. By comparison of HCl/HNO_3 and HCl/O_3 in the stratosphere with an air mass probed in the vicinity of the subtropical jet, we describe the state of mixing and discuss the location of a mixing layer [*Fischer et al.*, 2000] relative to the dynamical and the thermal tropopause. While *Marcy et al.* [2004] discuss transport of stratospheric O_3 into the upper troposphere, we extend the method to altitudes above the tropopause to determine the tropospheric content in the stratosphere. Additionally, we include a second mainly stratospheric tracer HNO_3 in our analysis and compare the different mixing states in a region of enhanced isentropic transport. A quantitative composition analysis in the Extratropical Transition Layer (ExTL) is performed.

2. The Atmospheric Chemical Ionization Mass Spectrometer

The Atmospheric chemical Ionization Mass Spectrometer (AIMS) is a newly designed CIMS instrument, operated with an electrical discharge source and in-flight calibration. In contrast to earlier measurements using radioactive sources for ionization [*Marcy et al.*, 2005; *Jurkat et al.*, 2010], SF_5^- reagent ions are produced by an electrical discharge between a gold needle tip and a circular pin hole at the upstream part of the flow reactor. The reagent ions are instantaneously mixed in the flow tube with the sample flow generating stable product ions by fluoride transfer. Product and reagent ions are detected at a rate of 1 Hz by a linear quadrupole and a channeltron housed inside a differentially pumped vacuum chamber. Sensitivity of the instrument and possible absorption effects on the walls are monitored using an in-flight online calibration with isotopically labeled SO_2, which was also measured but will not be shown here. The relative sensitivity and stability for HCl and HNO_3 are likewise monitored and are stable within named measurement errors over the whole flight on 4 September 2012. For an absolute calibration, two pressure- and temperature-controlled permeation ovens are used to generate standards for HCl and HNO_3 calibration. The backward facing trace gas inlet mounted on the central fuselage of the aircraft is equipped with a 1/2" heated perfluoroalkoxy (PFA) tube ($T = 40°C$). A high bypass flow of 4.7 slm maintained at ambient pressure is achieved by an additional scroll pump. A smaller flow of 1.1 slm enters the mass spectrometer through a PFA pressure control valve. Background measurements are hourly performed by flushing the inlet with dry synthetic air. The 1σ detection limit of the instrument for both HCl and HNO_3 was between 10 and 15 parts per trillion by volume (pptv) during the campaign with a running mean over 20 data points and for atmospheric $H_2O < 100$ ppmv. A systematical error is estimated to be between 18 and 25%. The reagent ions additionally allow detection of nitrous acid (HONO) [*Voigt et al.*, 2010; *Jurkat et al.*, 2011] and chlorine nitrate ($ClONO_2$) [*Marcy et al.*, 2005], which are not considered here. In addition, the instrument can be used to measure high concentrations of tropospheric HCl, HNO_3, and SO_2 in volcanic plumes [*Voigt et al.*, 2014]. O_3 mixing ratios were measured at a rate of 10 Hz with high precision and reproducibility of 0.5% and 1.5% using a combination of a chemiluminescence sensor and an UV photometer [*Zahn et al.*, 2012]. The instrument measuring CO is based on the three-channel tunable diode laser instrument for atmospheric research used during SPURenstofftransport in der Tropopausenregion (SPURT) [*Hoor et al.*, 2004]. With a new quantum cascade laser setup, we achieved a short-term precision of 0.9 ppbv at 1.5 s integration time and an upper limit for the total uncertainty of 2.3 ppbv without any corrections applied.

3. In Situ Measurements of HCl and HNO_3 in the Tropopause Region

The TACTS/ESMVal mission comprised 13 flights from latitudes of 68°N to 65°S and 25°E to 74°W with more than 120 flight hours. The aim of the campaign was to study the transport and composition of the UT/LMS region and provide observations for global climate model validation.

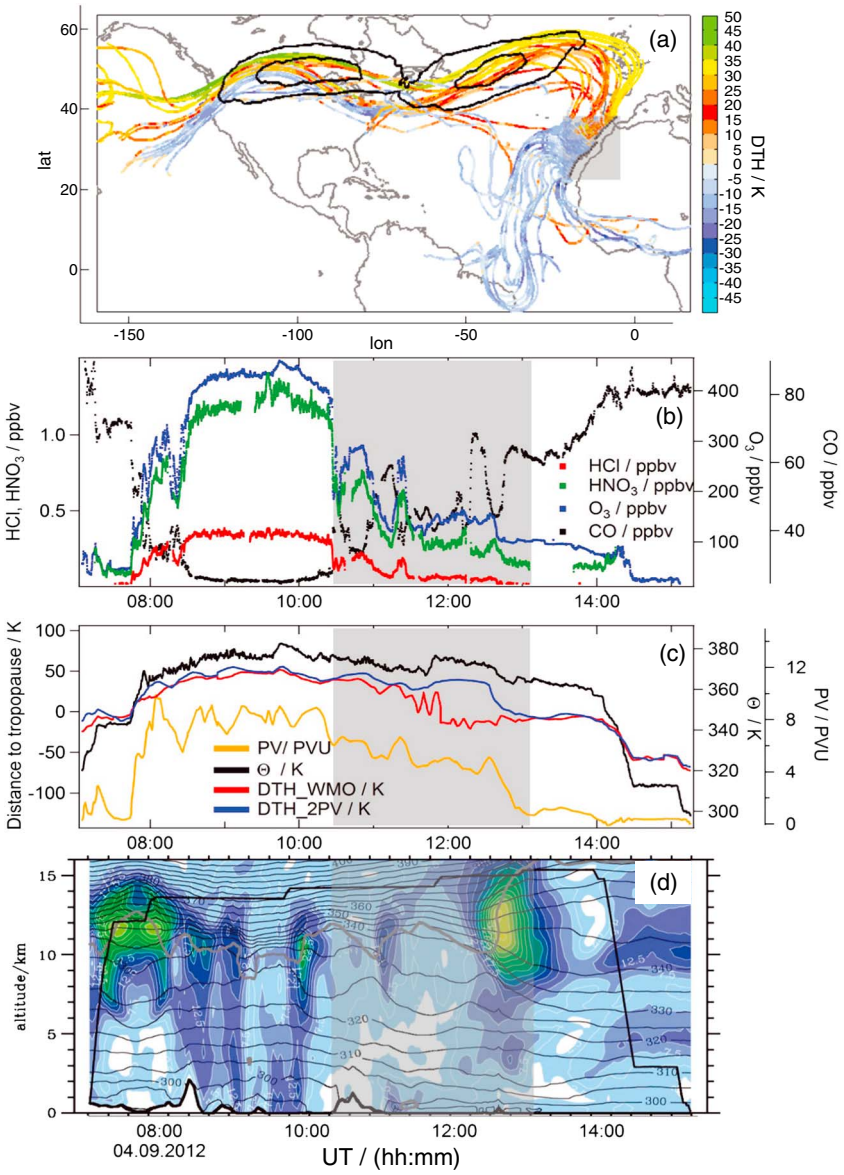

Figure 1. (a) Flight track of HALO on 4 September 2012 and 10-day backward trajectories ending on the flight track, color coded with the distance to the thermal tropopause (DTH). In the vicinity of the subtropical jet at 26°N (grey-shaded area), the backward trajectories show a change in air mass origin from stratospheric (DTH > 0) to tropospheric values when the aircraft flew from high to low latitudes. The black contour lines show mean zonal wind velocities of 20 and 25 m/s during the 10 day period. (b) Trace gas mixing ratios of HCl (red), HNO_3 (green), O_3 (blue), and CO (black) measured on 4 September 2012 together with the HALO cruise altitude. The grey-shaded area corresponding to Figure 1a marks the mixed air mass. (c) Potential temperature (θ, black) derived from onboard HALO measurements together with calculated measured concentration in potential vorticity (PV, yellow) from operational ECMWF data, the distance to the thermal (DTH_WMO, red), and dynamical tropopause (DTH_2PV, blue), respectively. (d) The color code shows horizontal wind velocities (white $\leq$ 2.5 m/s to light green 32 m/s, in steps of 2.5 m/s) as a curtain along the flight track derived from ECMWF analysis. Grey contours are potential temperature isolines, in black the flight altitude and in light grey the dynamical tropopause (2 PVU) are shown. At approximately 12:00 UT, the aircraft entered a region with enhanced horizontal wind velocities.

In this paper we concentrate on one flight performed on 4 September 2012 going from Oberpfaffenhofen, Germany, to Sal, Cape Verde. In Figure 1a, the flight track and 10-day backward trajectories run with the Lagrangian Analysis Tool LAGRANTO [*Wernli and Davies*, 1997] based on operational ECMWF data are shown. Using these trajectory calculations, we derive the most recent contact to the stratosphere for air masses sampled below the tropopause. Figures 1b and 1c show the time series of HCl, HNO_3, O_3 and CO

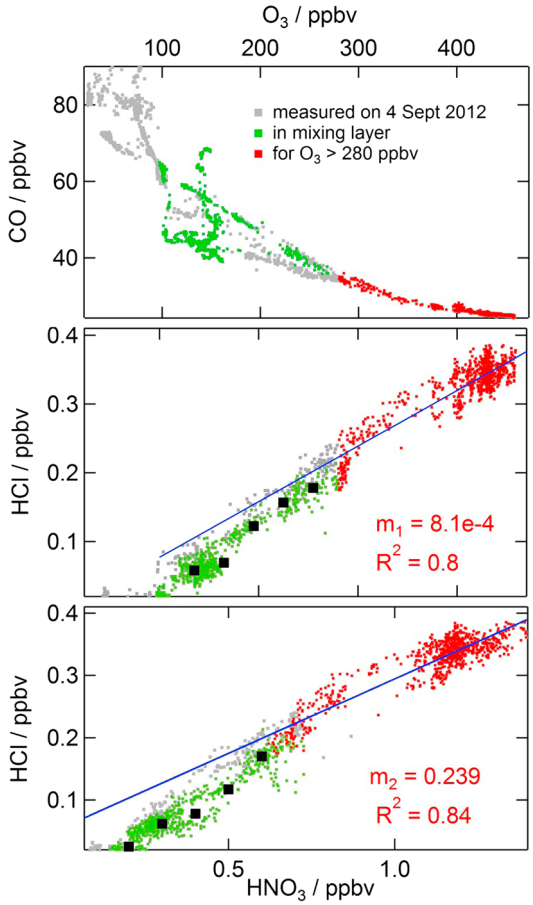

Figure 2. Scatterplots of 10 s averaged mole fractions of CO vs O_3, HCl vs O_3, and HCl vs HNO_3. A tight correlation (R^2 = 0.8 and 0.84) is observed for all stratospheric tracers in the unperturbed lower stratosphere (red, O_3 > 280 ppbv). The stratospheric fit curves with slopes m_1 and m_2 are colored in blue. Data marked in green correspond to the grey-shaded area in Figure 1 and were collected in the vicinity of the subtropical jet. Black squares represent the median of 30 ppbv O_3 and 0.1 ppbv HNO_3 bins for O_3 < 280 ppbv.

together with flight altitude, potential temperature (θ), vertical distance to the thermal (DTH_WMO) and the dynamical tropopause (DTH_2PV), measured in potential temperature and the potential vorticity along the flight path. The dynamical tropopause is represented by the 2 PVU-isoline in the extratropics and the 380 K-isentrope in the tropics. The thermal tropopause is calculated according to the WMO definition based on the standard lapse rate. Within the 8.5 h flight both tropospheric and stratospheric air was encountered, from 20 K below the tropopause to 57 K above the tropopause, and potential temperatures between 300 and 382 K. Tropospheric background mixing ratios of HCl encountered at 7:50 UT and after 13:20 UT are below the detection limit of 15 pptv. This lack of HCl has been observed during most flights and confirms the exclusive stratospheric origin of upper tropospheric HCl in the absence of recent volcanic eruptions. In the following discussion we focus on the trace gas relation in the grey-shaded area. Here PV is dropping from stratospheric (6 PVU) to tropospheric values (1 PVU). Figure 1d shows the horizontal wind velocities (color coded) in a vertical curtain plot along the flight route. The STJ is represented by high horizontal wind velocities with maximum values of 32 m/s in the center of the jet. The high horizontal wind speeds are extending deep into the stratosphere where HALO sampled at the upper edge of these extensions. Isentropes are crossing the dynamical tropopause indicating a potential pathway of cross-tropopause trace gas transport. Comparison of the thermal and the dynamical tropopause in the vicinity of the STJ reveals the largest potential temperature difference up to 57 K, with the dynamical tropopause 38 K below the aircraft and the thermal tropopause at a distance of 19 K above. To study the effects of mixing of tropospheric and stratospheric air, we use the tropopause definitions and tracer-tracer correlations of HCl to O_3 and HCl to HNO_3.

4. Stratospheric Tracer-Tracer Coordinates

Tracer-tracer coordinates are commonly used to study the chemical transition from troposphere to stratosphere. While some studies apply CO as a tropospheric marker and O_3 as a stratospheric marker [*Zahn et al.*, 2000; *Hoor et al.*, 2004], we focus on the relationship of two stratospheric tracers [*Marcy et al.*, 2004]. To support our analysis we use the tropospheric tracer CO. Figure 2 shows scatterplots of CO to O_3, HCl to O_3 and HCl to HNO_3 for the flight on 4 September 2012. While the branching of the CO-O_3 correlation and the large CO variability between 100 and 280 ppb O_3 indicate mixing between tropospheric and stratospheric air, the scatterplots of the stratospheric tracers show a compact linear relationship. To separate the characteristic, unperturbed stratospheric background from the mixing layer, slopes for different O_3 ranges have been derived. By computing the slopes for lower O_3 cutoff values between 100 and 350 ppbv in steps of 50 ppbv, a change of the slope of 15% for the fit of all data points as compared to the fit for O_3 > 280 ppbv was observed. The change in the slope will be used here as an independent criterion to derive the upper

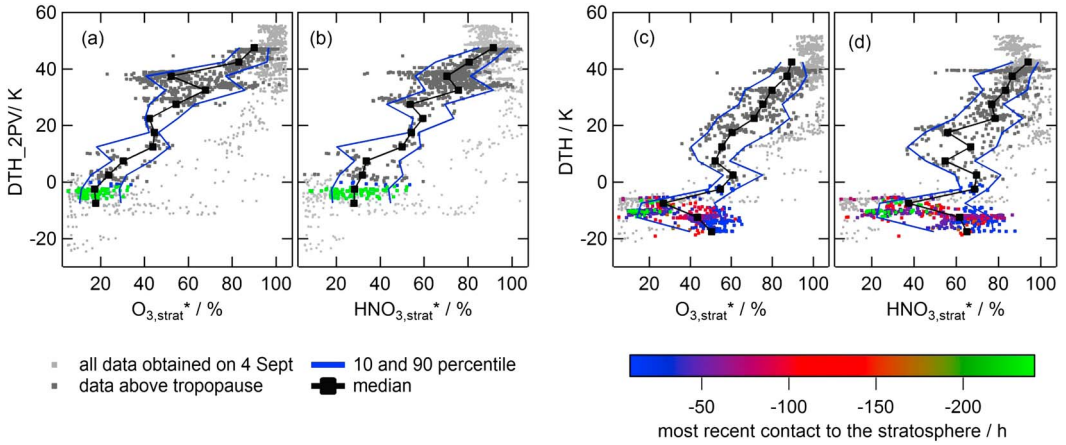

Figure 3. The relative stratospheric contributions $O^*_{3,strat}$ and $HNO^*_{3,strat}$ and the 5 K percentiles (median (black squares), 10th and 90th (dark blue lines)) plotted against the distance to the (a, b) dynamical and (c, d) thermal tropopause are shown. Colored in light grey are data of the entire flight. The dark grey-colored data represent the mixed air mass above the tropopause. Data below the thermal tropopause have been color coded with the trajectory based analysis of the most recent contact to the stratosphere (in hours). Light green colored is air with the most recent contact to the stratosphere ≥ 240 h.

boundary of the mixing layer equivalent to the lower boundary of the unperturbed lower stratosphere. The boundary is consistent with a broadening of the stratospheric branch in the CO-O_3 tracer-tracer space below 280 ppbv O_3. The linear fits for the unperturbed stratospheric branch (data with $O_3 > 280$ ppbv) yield high correlation coefficients of $R^2 = 0.8$ and 0.84, with a slope of $m_1 = 8.1 \times 10^{-4}$ for the HCl and O_3 correlation and a slope of $m_2 = 0.239$ for the fit of HCl and HNO_3.

The data within the grey-shaded area in Figure 1 are green colored in Figure 2. They show a systematic lower ratio of HCl and O_3 and HCl and HNO_3 than the corresponding ratio on the extrapolated stratospheric fit curve (blue fit line). Additionally, the fits for the correlations of tracers sampled in the mixing layer have significantly higher slopes of 1×10^{-3} for HCl/O_3 and 0.324 for HCl/HNO_3.

In the following discussion, X represents the mole fraction of either O_3, HNO_3, or HCl in the mixed (index M) air mass, and the stratospheric (index S) and tropospheric (index T) end-members, respectively. The index *strat* is used for the stratospheric content X_{strat} of the observed mole fraction X_M in the mixed air mass, thus $X_M = X_{strat} + X_{trop}$. We assume linear mixing of air along a mixing line between a stratospheric end-member ratio HCl_S/X_S located on the stratospheric fit curve and an upper tropospheric end-member ratio HCl_T/X_T with $HCl_T = 0$. Thus, we derive the stratospheric content X_{strat} based on *Marcy et al.* [2004]:

$$X_{strat} = \frac{HCl_M}{HCl_S} X_S \quad (1)$$

and $X^*_{strat} = X_{strat}/X_M$ is the relative stratospheric content. To calculate X_{strat}, we use the stratospheric end-member at the lower end of the stratospheric fit curve. The choice of the end-member implies that the stratospheric part in the mixed air mass originated from the lower boundary of the unperturbed stratosphere. For our calculation we use the stratospheric end-member at $O_{3,S} = 280$ ppbv and $HNO_{3,S} = 0.63$ ppbv, closest to the ratios in the mixed air mass in the tracer-tracer space, with $HCl_S/O_{3,S} = 7.9 \times 10^{-4}$ and $HCl_S/HNO_{3,S} = 0.318$.

5. Two-Way Transport Across the Tropopause

The vertical profiles of $O^*_{3,strat}$ and $HNO^*_{3,strat}$ with respect to the dynamical (Figures 3a and 3b) and the thermal tropopause (Figures 3c and 3d) are shown. For a clearer picture of the profiles and to minimize the influence of small-scale variability, the median, the 10th, and 90th percentiles are calculated for 5 K bins in the vertical.

The mixed air mass marks a distinct transition layer between pure tropospheric (0% X^*_{strat}) and pure stratospheric air (100% X^*_{strat}). The stratospheric content ranges between 20% and 100% for $O^*_{3,strat}$ and 30% and

100% for $HNO^*_{3,strat}$. It is decreasing with decreasing distance from the tropopause. The air mass was sampled mostly above the dynamical but centered around the thermal tropopause at potential temperatures between 320 K and 370 K. Thus, mixed air with significant tropospheric content was detected above the thermal and dynamical tropopause and mixed air with stratospheric content below the thermal tropopause. For $O^*_{3,strat}$ and $HNO^*_{3,strat}$ below the thermal tropopause, different transport time scales, derived from trajectory analysis, can be distinguished: air with recent contact to the stratosphere corresponds to a higher stratospheric content of 60%–80% while air with the last contact to the stratosphere at more than 240 h before the measurement contains only 20%–30% of stratospheric O_3 and HNO_3. By using the HCl-tagged air, we can unambiguously distinguish the stratospheric contribution to the upper tropospheric HNO_3 and O_3 budget with additional information of the time of tropopause crossing from backward trajectory calculations. Thus, we see mixing in the vicinity of the STJ affecting the ExTL up to 30–40 K above the low extratropical thermal tropopause. The difference in the mixing state between the two profiles arises from the different sources and background concentrations of upper tropospheric O_3 as compared to upper tropospheric HNO_3 and the difference in gradients across the tropopause. Tropospheric air with low O_3 is mixed into the stratosphere with generally high O_3 mole fractions. After mixing the stratospheric air exhibits a reduced O_3 concentration and is therefore diluted with respect to O_3. Due to different gradients of O_3 and HNO_3, the stratospheric air mass experiences a stronger dilution of the O_3 concentration than dilution of HNO_3 concentration.

6. Discussion

Using tracer-tracer correlations to study mixing demands an analysis of the stability and lifetime of the trace gases compared to the mixing time scales. The following discussion focuses on the instrumental and atmospheric parameters affecting the analysis. Generally, the deviation of HCl/O_3 from the stratospheric ratio may have three independent reasons which may all influence the ratio: (1) mixing of tropospheric with stratospheric air, (2) solution of HCl and HNO_3 in liquid water droplets, and (3) heterogeneous reactions on cirrus cloud ice particles, e.g., trapping of HNO_3. HCl activation on cirrus clouds may cause a reduction in the concentration of up to 50% but only for high particulate surface areas [*Thornton et al.*, 2007]; these are rarely observed in the stratosphere. Trapping and burial of HNO_3 in tropical cirrus cloud particles, potentially leading to a small depletion in the gas phase with subsequent vertical redistribution, have been observed in the tropical tropopause. A climatology and overview are given in *Voigt et al.* [2006]. In the present case, the slope of the two trace gas correlations is shifted and tilted when compared to the stratospheric slope but it is still a relative compact mixing line with correlation coefficients of $R^2 = 0.89$ and 0.9. In case of chemical or microphysical removal of either component, the compactness would have suffered. Therefore, we argue that mixing is mainly responsible for the observed shift in the ratios of the trace gases.

The criteria for the choice of the stratospheric end-members leave some uncertainty to the method. To compare the range of potential end-members, we investigated the variability in the stratosphere and in the troposphere; here O_3 is used as an example. The slope of the stratospheric fit curve represents an upper limit of potential stratospheric end-members of $HCl_S/O_{3,S} = 8.1 \times 10^{-4}$. The lower limit is given for O_3 at 280 ppbv with $HCl_S/O_{3,S} = 7.9 \times 10^{-4}$. The choice of this end-member is also supported by a broadening of the stratospheric branch in the CO/O_3 correlation. The respective tropospheric end-members $O_{3,T}$ are on average 104 ± 26 ppbv, thus within the expected range for typical upper tropospheric concentrations [*Murphy et al.*, 1993]. We examine the spread of potential tropospheric end-members by deriving the frequency of occurrence of $O_{3,T}$ for $HCl_T <$ detection limit and altitudes > 6 km for midlatitude measurements. The distribution was fitted by a gaussian fit with a mean of 74 ± 24 ppbv. Due to a smaller spread, the uncertainty for the calculation of X_{strat} is minimized by using a stratospheric end-member on the stratospheric fit curve.

A lower limit of stratospheric $O^*_{3,strat}$ and $HNO^*_{3,strat}$ that can be derived from this method is given by the detection limit of the HCl measurements. A detection limit of 15 pptv gives an uncertainty of 16 ppbv $O_{3,strat}$ and 0.05 ppbv $HNO_{3,strat}$. The relative uncertainty is largest at the lowest mixing ratios.

The slope m_1 of the stratospheric fit is higher than former measurements [*Marcy et al.*, 2004; *Jurkat et al.*, 2010], but the slopes agree within the named uncertainties of both measurements. The deviation may also partly evolve from a latitude dependence of the ratio considering that *Marcy et al.* [2004] sampled at subtropical latitudes where O_3 is produced at a higher rate. The slopes m_1 and m_2 and therefore $HCl_S/O_{3,S}$

and $HCl_S/HNO_{3,S}$ for tropical regions may be smaller which would result in an underestimation of the stratospheric content X_{strat}.

7. Summary and Outlook

In this paper we present a new method to quantify the stratospheric content of HNO_3 and O_3 in a mixing layer above and below the tropopause with stratospheric tracer-tracer correlation analysis. High-resolution airborne measurements of HCl and HNO_3 in the UT/LMS have been conducted with the AIMS instrument onboard the new research aircraft HALO during the TACTS/ESMVal Mission. The mixed layer was observed at low concentrations of HCl, HNO_3, and O_3 up to 30 K above the thermal and dynamical tropopause in the ExTL. The profiles of O_3 and HNO_3 show an increasing tropospheric content with decreasing distance from the tropopause. We propose to use the ratios HCl/O_3 and HCl/HNO_3 as a good proxy to study quantitatively the effects of mixing in the ExTL. Additionally, upper tropospheric O_3 and HNO_3 from local or remote sources can be differentiated from downward transported stratospheric O_3 and HNO_3. Future analysis will focus on regional and seasonal variability of mixing and transport of these and other stratospheric tracers in the ExTL. Our measurements extend data from remote sensing instruments on satellites in the lower stratosphere to lower altitudes and better resolutions.

Acknowledgments

TACTS/ESMVal was funded by the DFG SPP-HALO 1294 and the DLR-Project ESMVal. Part of the work was funded by HGF contract VH-NG-309. Further, we thank the DLR flight department for their excellent support during the campaign.

The Editor thanks two anonymous reviewers for their assistance in evaluating this paper.

References

Fischer, H., F. G. Wienhold, P. Hoor, O. Bujok, C. Schiller, P. Siegmund, M. Ambaum, H. A. Scheeren, and J. Lelieveld (2000), Tracer correlations in the northern high latitude lowermost stratosphere: Influence of cross-tropopause mass exchange, *Geophys. Res. Lett.*, *27*(1), 97–100, doi:10.1029/1999GL010879.

Haynes, P., and E. Shuckburgh (2000), Effective diffusivity as a diagnostic of atmospheric transport: 1. Stratosphere, *J. Geophys. Res.*, *105*(D18), 22,777–22,794, doi:10.1029/2000JD900093.

Hegglin, M. I., C. D. Boone, G. L. Manney, and K. A. Walker (2009), A global view of the extratropical tropopause transition layer from atmospheric chemistry experiment fourier transform spectrometer O_3, H_2O, and CO, *J. Geophys. Res.*, *114*, D00811, doi:10.1029/2008JD009984.

Hoor, P., C. Gurk, D. Brunner, M. I. Hegglin, H. Wernli, and H. Fischer (2004), Seasonality and extent of extratropical TST derived from in-situ CO measurements during SPURT, *Atmos. Chem. Phys.*, *4*, 1427–1442, doi:10.5194/acp-4-1427-2004.

Jurkat, T., C. Voigt, F. Arnold, H. Schlager, H. Aufmhoff, J. Schmale, J. Schneider, M. Lichtenstern, and A. Dörnbrack (2010), Airborne stratospheric ITCIMS measurements of SO_2, HCl, and HNO_3 in the aged plume of volcano Kasatochi, *J. Geophys. Res.*, *115*, D00L17, doi:10.1029/2010JD013890.

Jurkat, T., C. Voigt, F. Arnold, H. Schlager, J. Kleffmann, H. Aufmhoff, D. Schäuble, M. Schaefer, and U. Schumann (2011), Measurements of HONO, NO, NO_y and SO_2 in aircraft exhaust plumes at cruise, *Geophys. Res. Lett.*, *38*, L10807, doi:10.1029/2011GL046884.

Marcy, T., R. Gao, M. Northway, P. Popp, H. Stark, and D. Fahey (2005), Using chemical ionization mass spectrometry for detection of HNO_3, HCl, and $ClONO_2$ in the atmosphere, *Int. J. Mass Spectrom.*, *243*(1), 63–70, doi:10.1016/j.ijms.2004.11.012.

Marcy, T. P., et al. (2004), Quantifying stratospheric ozone in the upper troposphere with in situ measurements of HCl, *Science*, *304*(5668), 261–265, doi:10.1126/science.1093418.

Murphy, D. M., D. W. Fahey, M. H. Proffitt, S. C. Liu, K. R. Chan, C. S. Eubank, S. R. Kawa, and K. K. Kelly (1993), Reactive nitrogen and its correlation with ozone in the lower stratosphere and upper troposphere, *J. Geophys. Res.*, *98*(D5), 8751–8773, doi:10.1029/92JD00681.

Pan, L. L., W. J. Randel, J. C. Gille, W. D. Hall, B. Nardi, S. Massie, V. Yudin, R. Khosravi, P. Konopka, and D. Tarasick (2009), Tropospheric intrusions associated with the secondary tropopause, *J. Geophys. Res.*, *114*, D10302, doi:10.1029/2008JD011374.

Riese, M., F. Ploeger, A. Rap, B. Vogel, P. Konopka, M. Dameris, and P. Forster (2012), Impact of uncertainties in atmospheric mixing on simulated UTLS composition and related radiative effects, *J. Geophys. Res.*, *117*, D16305, doi:10.1029/2012JD017751.

Thornton, B. F., et al. (2007), Chlorine activation near the midlatitude tropopause, *J. Geophys. Res.*, *112*, D18306, doi:10.1029/2006JD007640.

Voigt, C., H. Schlager, H. Ziereis, B. Kärcher, B. P. Luo, C. Schiller, M. Krämer, P. J. Popp, H. Irie, and Y. Kondo (2006), Nitric acid in cirrus clouds, *Geophys. Res. Lett.*, *33*, L05803, doi:10.1029/2005GL025159.

Voigt, C., et al. (2010), In-situ observations of young contrails: Overview and selected results from the CONCERT campaign, *Atmos. Chem. Phys.*, *10*(18), 9039–9056.

Voigt, C., P. Jessberger, T. Jurkat, S. Kaufmann, R. Baumann, H. Schlager, N. Bobrowski, G. Guffirda, and G. Salerno (2014), Evolution of SO_2, HCl, HNO_3 and CO_2 in the volcanic plume from Etna, *Geophys. Res. Lett.*, doi:10.1002/2013GL058974.

Wernli, H., and H. C. Davies (1997), A lagrangian-based analysis of extratropical cyclones. I: The method and some applications, *Q. J. R. Meteorol. Soc.*, *123*(538), 467–489, doi:10.1002/qj.49712353811.

WMO, W. M. O. (2010), Scientific assessment of ozone depletion: 2010, *WMO Rep. 52*, World Meteorol. Org., Geneva, Switzerland.

Zahn, A., et al. (2000), Identification of extratropical two-way troposphere-stratosphere mixing based on CARIBIC measurements of O_3, CO, and ultrafine particles, *J. Geophys. Res.*, *105*(D1), 1527–1535, doi:10.1029/1999JD900759.

Zahn, A., J. Weppner, H. Widmann, K. Schlote-Holubek, B. Burger, T. Kühner, and H. Franke (2012), A fast and precise chemiluminescence ozone detector for eddy flux and airborne application, *Atmos. Meas. Tech.*, *5*(2), 363–375, doi:10.5194/amt-5-363-2012.